HHS Public Access

Author manuscript

Funct Imaging Model Heart. Author manuscript; available in PMC 2023 July 18.

Published in final edited form as:

Funct Imaging Model Heart. 2023 June ; 13958: 34–43. doi:10.1007/978-3-031-35302-4_4.

A Micro-anatomical Model of the Infarcted Left Ventricle Border Zone to Study the Influence of Collagen Undulation

Emilio A. Mendiola[1], **Eric Wang**[1], **Abby Leatherman**[1], **Qian Xiang**[2], **Sunder Neelakantan**[1], **Peter Vanderslice**[2], **Reza Avazmohammadi**[1,3,4]

[1]Department of Biomedical Engineering, Texas A&M University, College Station, TX, USA

[2]Department of Molecular Cardiology, Texas Heart Institute, Houston, TX, USA

[3]J. Mike Walker '66 Department of Mechanical Engineering, Texas A&M University, College Station, TX, USA

[4]Department of Cardiovascular Sciences, Houston Methodist Academic Institute, Houston, TX, USA

Abstract

Myocardial infarction (MI) results in cardiac myocyte death and often initiates the formation of a fibrotic scar in the myocardium surrounded by a border zone. Myocyte loss and collagen-rich scar tissue heavily influence the biomechanical behavior of the myocardium which could lead to various cardiac diseases such as systolic heart failure and arrhythmias. Knowledge of how myocyte and collagen micro-architecture changes affect the passive mechanical behavior of the border zone remains limited. Computational modeling provides us with an invaluable tool to identify and study the mechanisms driving the biomechanical remodeling of the myocardium post-MI. We utilized a rodent model of MI and an image-based approach to characterize the three-dimensional (3-D) myocyte and collagen micro-architecture at various timepoints post-MI. Left ventricular free wall (LVFW) samples were obtained from infarcted hearts at 1-week and 4-week post-MI (n = 1 each). Samples were labeled using immunoassays to identify the extracellular matrix (ECM) and myocytes. 3-D reconstructions of the infarct border zone were developed from confocal imaging and meshed to develop high-fidelity micro-anatomically accurate finite element models. We performed a parametric study using these models to investigate the influence of collagen undulation on the passive micromechanical behavior of the myocardium under a diastolic load. Our results suggest that although parametric increases in collagen undulation elevate the strain amount experienced by the ECM in both early- and late-stage MI, the sensitivity of myocytes to such increases is reduced from early to late-stage MI. Our 3-D micro-anatomical modeling holds promise in identifying mechanisms of border zone maladaptation post-MI.

Keywords

cardiac remodeling; border zone; myocardial infarction; confocal imaging; finite element modeling

rezaavaz@tamu.edu .

1 Introduction

Myocardial infarction (MI), caused by a lack of sufficient blood flow to the ventricular myocardium, results in cardiac myocyte death and often initiates the formation of fibrotic scar tissue in the left ventricle free wall (LVFW). In the weeks following MI, several remodeling events occur in the left ventricle (LV) myocardium inducing substantial changes in LVFW biomechanical behavior [12]. The biomechanical behavior of the LVFW, informed by structural and compositional remodeling post-MI, has been indicated as an essential determinant of the long-term functional outcome of the LV post-MI [2]. As such, there is a need to study the link between structural remodeling and the biomechanical behavior of the LV with the aim of better understanding the interaction between the two.

Given the established link between LVFW biomechanical behavior and the organ-level function [10], post-MI LV remodeling has been studied extensively. However, previous studies have focused on characterizing the remodeling of the scar region at the tissue scale [2,4] and the knowledge of the micro-environment of infarcted myocardium, in particular the infarct border zone, remains elusive. In particular, the effect of collagen fiber undulation, which governs the point at which collagen fibers are fully recruited, has been overlooked. We hypothesize that multiscale computational modeling could be a tool used to improve the understanding of the micromechanical environment in the border zone and advance the understanding of the link between microstructural remodeling in the border zone and organ-level function.

To form an understanding of the effect of collagen undulation on the micromechanical behavior of the infarcted LV myocardium, we have developed 3-D finite element (FE) models of the infarct border zone that incorporate accurate micro-anatomical structures of the myofibers (myocytes) from high-resolution confocal imaging of the microscale samples of the border zone (Fig. 1). Models were developed from 3-D imaging datasets from infarcted rat hearts at two timepoints (1-week and 4-week) post-MI. In this study, we simulated the mechanical behavior of these 3-D micro-anatomical models under biaxial stresses, representing enddiastolic loading, and quantified the myofiber and extracellular matrix (ECM) strain profiles. We then performed a parametric study to explore the effect of collagen undulation on the strains. Material properties used in the model were taken from an analytical fit to ex-vivo mechanical test data. Results from the present investigation improve the understanding of the micro-environment at early- and late-stage MI timepoints and can aid in identifying mechanisms driving border zone biomechanical remodeling.

2 Materials and Methods

2.1 Animal Model

The animals used in this work were treated in accordance with guidelines approved by the Institutional Animal Care and Use Committee (IACUC) at the Texas Heart Institute. Two male Wistar-Kyoto (WKY) rats, 8 weeks old at the start of the experiment, were used in this study. Anteriobasal infarct was induced in two rats (n = 2) by ligation of the left anterior descending artery near the base of the heart as previously described [11]. Animals were sacrificed at 1-week and 4-week post-MI, hereafter designated as 1-wk and 4-wk,

respectively. Immediately prior to sacrifice, LV hemodynamic and anatomical measurements were obtained via left heart catheterization and echocardiography.

2.2 Preparation and Labeling of Myocardium Samples

Hearts were excised, and the ventricles were perfused and stored in 4% paraformaldehyde (PFA) solution for 3 h. The ventricles were then washed with phosphate-buffered saline (PBS). Biopsies were incubated in 30% sucrose in PBS solution and frozen to prevent tissue damage. Full-thickness rectangular specimens of the full LVFW were isolated with slab edges being aligned with the longitudinal, circumferential, and radial directions of the LV. The slabs were then frozen in optimal cutting temperature compound (Sakura Finetek Europe B.V., Alphen aan den Rijn, Netherlands) and cryosectioned into 60-micron thick slices. Mid-wall slices were washed in PBS with 0.1% Triton X-100 (PBST) and fixed in a Pelco Biowave (Ted Pella, Inc., Redding, CA) laboratory microwave processor. The tissue underwent microwave irradiation for 2 min, washed in PBST with 3% bovine serum albumin (BSA). Using direct immunofluorescence, the tissue sections were labeled with Alpha-Smooth Muscle Actin (α-SMA) Monoclonal Antibody (1A4), eFluor 570, eBioscience™ for the myocytes. Alexa Fluor 647-conjugated anti-Vimentin antibodies were also applied at a concentration of 1:200. Each slice received 150 μL of antibody solution and was covered in parafilm. The tissues underwent microwave irradiation for 2 min followed by 5-minute rest, then were incubated for 8 h overnight, and then rinsed in PBS with microwave irradiation for 2 min. Next, wheat germ agglutinin (WGA)-conjugated Alexa Fluor 680 (Invitrogen, Carlsbad, California) was applied at 1:200 concentration, and each slide received 150 μL of antibody solution. DAPI (D3571, Thermo Fisher Scientific) at 1 μg/ml was distributed at 150 μL for each slide to label the nuclei. The slides were rinsed off and underwent microwave irradiation for 2 min in sodium phosphate buffer (50 mM, pH 7.0). Finally, slices were mounted in a glycerol-based medium (80% glycerol, with n-propyl gallate antifade) and allowed to dry before storing at −20 °C.

2.3 Confocal Microscopy Imaging

Prepared coverslips were imaged using a laser scanning confocal microscope Leica TCS SP8 with a 40x oil immersion objective at a resolution of 1024 × 1024 pixels and an image size of 204 × 204 μm with a voxel size of 0.196 × 0.196 × 0.333 μm. The infarct scar was identified as fibrotic tissue dense in collagen and without any myocytes. The remote region was identified far from the infarct scar, where only healthy myocytes and typical collagen structures are present. Finally, the border zone was recognized as the area between the infarct scar and the remote region where living and dead myocytes were both present [9]. A rotation of the field of view was applied before acquisition to yield a uniform myocyte orientation approximately parallel to the $\mathbf{e_1}$ axis (Fig. 2). 3-D image stacks were acquired to collect signals from DAPI, autofluorescence, WGA, α-SMA, and vimentin. Image stacks of 200–300 images covered the depth of each sample with a spacing of 200 nm between the images. To compensate for decreasing signal intensity at increased depths within the tissue, excitation compensation was applied by manually adjusting the laser intensity at points at various depths in the sample and linearly interpolating between them. The imaging software LAS X (version1.1.0 and higher, Leica) was used for this processing.

Slides were imaged at 40x using a compound microscope to obtain images of the collagen fibers. We quantified the undulation of collagen fiber bundles as the ratio of the distance between two endpoints of the bundle to the total length of the bundle such that the undulation parameter lies between 0 and 1. The extreme undulation values of 0 and 1 correspond to an entirely coiled and a perfectly straight fiber, respectively. Fiber undulation was converted to slack stretch for use in FE constitutive modeling by taking the slack stretch λ_s as the inverse of fiber undulation.

2.4 Finite-Element Model Development

Three-Dimensional Image Reconstruction.—3-D structures of myocytes and collagen fibers were reconstructed from confocal microscopy z-stack images of the border zone and analyzed using Imaris software. We applied median filters to reduce noise in the acquired image stacks and performed threshold cutoffs and background subtraction to enhance the contrast between the background and the target tissue. The image segmentation resulted in a 3-D representation of the individual myocytes and the extracellular space within the tissue sample (Fig. 2). The individually reconstructed myocytes were represented as a consol idated *myofiber* region. The two-region reconstruction, consisting of ECM and myofiber regions, was meshed in Mimics (Materialise, Leuven, Belgium), resulting in a volumetric mesh of ~85,000 linear tetrahedral elements.

Myofiber and Extracellular Matrix Constitutive Modeling.—The myofiber and ECM were modeled as hyperelastic, anisotropic, incompressible materials using constitutive models adapted from previous studies [6,7]. As individual myofiber orientations could be obtained directly from the imaging dataset, we defined the myofiber direction $\mathbf{f}_0$ as the predominant direction of the long axis of myofibers in the mesh, which was fairly constant throughout the sample with a splay of ±3.5°. The cross-fiber direction **s** was defined as the direction normal to the myofibers within the plane of the mesh.

The myofiber strain energy function (Ψ_{MYO}) was defined as a two-term invariant-based exponential constitutive form [5]. The form consisted of an isotropic matrix term stiffened by a primary fiber along $\mathbf{f}_0$ given by

$$\Psi_{MYO}(\mathbf{C}) = \frac{a}{2b}\left[e^{b(I_1-3)}-1\right] + \frac{a_m}{2b_m}\left[e^{b_m(I_4-1)^2}-1\right], \quad (1)$$

where **C** is the right Cauchy deformation tensor and the matrix term, involving $I_1 = tr(\mathbf{C})$ and the material properties of a and b, is related to the isotropic behavior of the myofiber regions. Also, $I_4 = \mathbf{f}_0 \cdot \mathbf{C}\mathbf{f}_0$ is equivalent to the square of the stretch along the fiber direction $\mathbf{f}_0$, and a_m and b_m characterize the transversely-isotropic behavior of the myofiber region.

Individual collagen fibers, having diameters at the scale of less than 1 μm, were bundled and consolidated together to constitute the ECM region. Similar to the case of myofiber, the ECM was modeled as an isotropic matrix reinforced by a primary fiber direction:

$$\Psi_{ECM}(\mathbf{C}) = \frac{a}{2b}\left[e^{b(I_1-3)}-1\right] + \frac{a_c}{2b_c}\left[e^{b_c\left(\frac{I_4}{\lambda_s^2}-1\right)^2}-1\right], \quad (2)$$

where, for simplicity, the constants related to the isotropic part were kept the same as those in the myofiber energy function, and a_c and b_c are, similarly, related to the anisotropic behavior of the ECM region. Given our interest in estimating myofiber and collagen contributions to myocardial mechanical behavior, we set $a = 0.22$ kPa and $b = 1.62$ as reference values, reflecting an inconsiderable mechanical contribution of the ground matrix in the LV myocardium [1,3], and let $\{a_m, b_m, a_c, b_c, \lambda_s\}$ to be the material parameter variables in this work. Although the chosen low values for a and b parameters are expected to lead to a minimal effect of the matrix term on the simulated LV biomechanical behavior, the inclusion of the matrix terms, involving I_1, in both Ψ_{MYO} and Ψ_{ECM}, was important to aid in the stabilization of the computational problem. Lastly, we note that the parameters $\{a, a_m, a_c\}$ have stress-like dimensions while $\{b, b_m, b_c\}$ are dimensionless. The constitutive parameters were estimated through an inverse problem approach via fitting an analytical solution for the full LVFW behavior to post-infarct biaxial data as described by Mendiola et al. [8]. The fitted parameters were used for parametric studies described below.

Finite-Element Biomechanical Simulations.—To better understand the effect of collagen undulation on the passive behavior of myocardial tissue in the scar border zone, we conducted a parametric study in which the slack stretch of the collagen fibers at each timepoint was varied, and the resulting alterations in regional strain were analyzed. First, the stress in the LVFW at the end-diastolic (ED) point was estimated via the Laplace law as

$$\sigma_{ED} = \frac{P_{ED}R_{ED}}{2t} \quad (3)$$

where P_{ED} is the ED pressure in Pascals, R_{ED} is the LV radius at ED in milimeters, and t is the LVFW thickness in milimeters. The 1-wk data used for these calculations were $P_{ED} = 1033.2$ Pa, $R_{ED} = 4.6$ mm $t = 1.47$ mm whereas the 4-wk data were $P_{ED} = 1080.7$ Pa, $R_{ED} = 4.6$ mm, $t = 1.22$ mm. These data were collected via LV catheterization and echocardiography immediately before sacrifice. The estimated ED wall stress was applied to the boundary surfaces of the FE model as a stress boundary condition. Initial simulations were run with the collagen slack length measured from imaging. Subsequent *in-silico* experiments were conducted using values for λ_s that were varied by ±5% and ±10%.

3 Results

The stress-strain response of the micro-anatomical models showed a stiffening behavior from 1-wk to 4-wk timepoints, similar to the biaxial test data [8]. Results are not presented here for brevity. At the maximum stress state, the strain in the $\mathbf{e}_1$ and $\mathbf{e}_2$ directions at both timepoints showed substantial heterogeneity throughout the model (Fig. 3). E_{11} tended to peak at the tips of the myocytes (noting that fiber directions were nearly aligned with $\mathbf{e}_1$) while E_{22} showed a more uniform distribution with the myocytes. Both strain components

exhibited higher values near the boundaries (compared to the central region of the volume) expected due to higher values of forces at the boundaries Fig. 3).

Varying collagen undulation in the ECM resulted in distinct regional strain behavior at each timepoint. The ECM accommodated greater strain than the myocytes at both timepoints (Fig. 4). A similar trend was noted in the ECM strain response versus undulation in both 1-wk and 4-wk models: larger strain was exhibited in the ECM as the slack stretch increased. In contrast, the 1-wk myocytes accommodated a larger strain than the 4-wk myocytes, and the 1-wk myocyte strain was noted to be more sensitive to the alterations in collagen fiber undulation than the 4-wk myocytes.

4 Discussion

In this study, we have developed a micro-anatomically accurate FE model of infarcted left ventricular myocardium based on a high-resolution imaging dataset. We used a structurally motivated constitutive modeling approach to quantify the microscale strain fields in the tissue and investigate the effect of collagen undulation on the micromechanical behavior of the infarct border zone.

Interestingly, results indicate that the ECM of the border zone accommodates greater strain than the myofibers in both early- and late-stage MI. We hypothesize that this observation is a result of (i) a greater concentration of collagen within the border zone samples and (ii) the slack behavior of the collagen fibers in the ECM, allowing for the strain to develop prior to the development of large tensile forces in the fibers. The parametric study conducted regarding the effect of the slack stretch on regional strain shows the myofibers in the 1-wk model accommodate greater strain under diastolic loading than do the 4-wk myofibers. This is consistent with previous studies indicating early post-MI myocardium is more compliant than late MI myocardium, resulting in generally better diastolic and systolic organ-level function [8]. Additionally, the kinematic behavior of 1-wk myofibers is more sensitive to alterations in collagen slack stretch. These results imply that, in addition to the cellular-level structure and composition of the border zone myocardium, collagen undulation acts as an important contributor to regional kinematic behavior. As such, further investigation of the timecourse alterations in collagen undulation post-MI and its influence on tissue- and organ-level function is warranted.

The model presented in this work offers improved histological and imaging processes to simulate the micro-environment of the infarcted LV. Such work is necessary to better understand the elusive link between cellular-level remodeling and organ-level function post-MI. Our modeling results have indicated that the diastolic kinematic behavior of the scar border zone is highly heterogeneous and is a function of various structural and biomechanical remodeling processes, including collagen fiber undulation. Future work will focus on the development of similar micro-structurally informed models capable of connecting our cellular-level predictions with tissue- and organ-level behaviors. Ultimately, our micro-anatomical modeling approach will allow for the connection of multiscale post-MI remodeling events and potentially aid in the identification of fiber-level remodeling events driving the transition of the MI to heart failure.

Acknowledgements.

This research was supported by the NIH Grant No. R00HL138288 to R.A.

References

1. Babaei H, et al. : A machine learning model to estimate myocardial stiffness from EDPVR. Sci. Rep 12(5433) (2022). 10.1038/s41598-022-09128-6
2. Fomovsky G, Thomopoulos S, Holmes J: Contribution of extracellular matrix to the mechanical properties of the heart. J. Mol. Cell. Cardiol 48(3), 490–496 (2010) [PubMed: 19686759]
3. Gao H, Li WG, Cai L, Berry C, Luo XY: Parameter estimation in a Holzapfel–Ogden law for healthy myocardium. J. Eng. Math 95(1), 231–248 (2015). 10.1007/s10665-014-9740-3 [PubMed: 26663931]
4. Holmes JW, Borg TK, Covell JW: Structure and mechanics of healing myocardial infarcts. Annu. Rev. Biomed. Eng 7(1), 223–253 (2005). 10.1146/annurev.bioeng.7.060804.100453 [PubMed: 16004571]
5. Holzapfel GA, Ogden RW: Constitutive modelling of passive myocardium: a structurally based framework for material characterization. Philos. Trans. R. Soc. Lond. A: Math. Phys. Eng. Sci 367(1902), 3445–3475 (2009). 10.1098/rsta.2009.0091
6. Li DS, Mendiola EA, Avazmohammadi R, Sachse FB, Sacks MS: A multi-scale computational model for the passive mechanical behavior of right ventricular myocardium. J. Mech. Behav. Biomed. Mater 142, 105788 (2023). 10.1016/j.jmbbm.2023.105788 [PubMed: 37060716]
7. Li DS, Mendiola EA, Avazmohammadi R, Sachse FB, Sacks MS: A high-fidelity 3D micromechanical model of ventricular myocardium. In: Ennis DB, Perotti LE, Wang VY (eds.) FIMH 2021. LNCS, vol. 12738, pp. 168–177. Springer, Cham (2021). 10.1007/978-3-030-78710-317
8. Mendiola EA, et al. : Contractile adaptation of the left ventricle post-myocardial infarction: predictions by rodent-specific computational modeling. Ann. Biomed. Eng 16(2), 721–729 (2022)
9. Mendiola EA, et al. : Identification of infarct border zone using late gadolinium enhanced MRI in rats. FASEB J. 36(S1) (2022). 10.1096/fasebj.2022.36.S1.R6220
10. Richardson WJ, Clarke SA, Quinn TA, Holmes JW: Physiological implications of myocardial scar structure. Compr. Physiol 5(4), 1877–1909 (2018). 10.1002/cphy.c140067
11. Samsamshariat SA, Samsamshariat ZA, Movahed MR: A novel method for safe and accurate left anterior descending coronary artery ligation for research in rats. Cardiovasc. Revasc. Med 6(3), 121–123 (2005). 10.1016/j.carrev.2005.07.001 [PubMed: 16275608]
12. Sutton MGSJ, Sharpe N: Left ventricular remodeling after myocardial infarction: pathophysiology and therapy. Circulation 101(25), 2981–2988 (2000) [PubMed: 10869273]

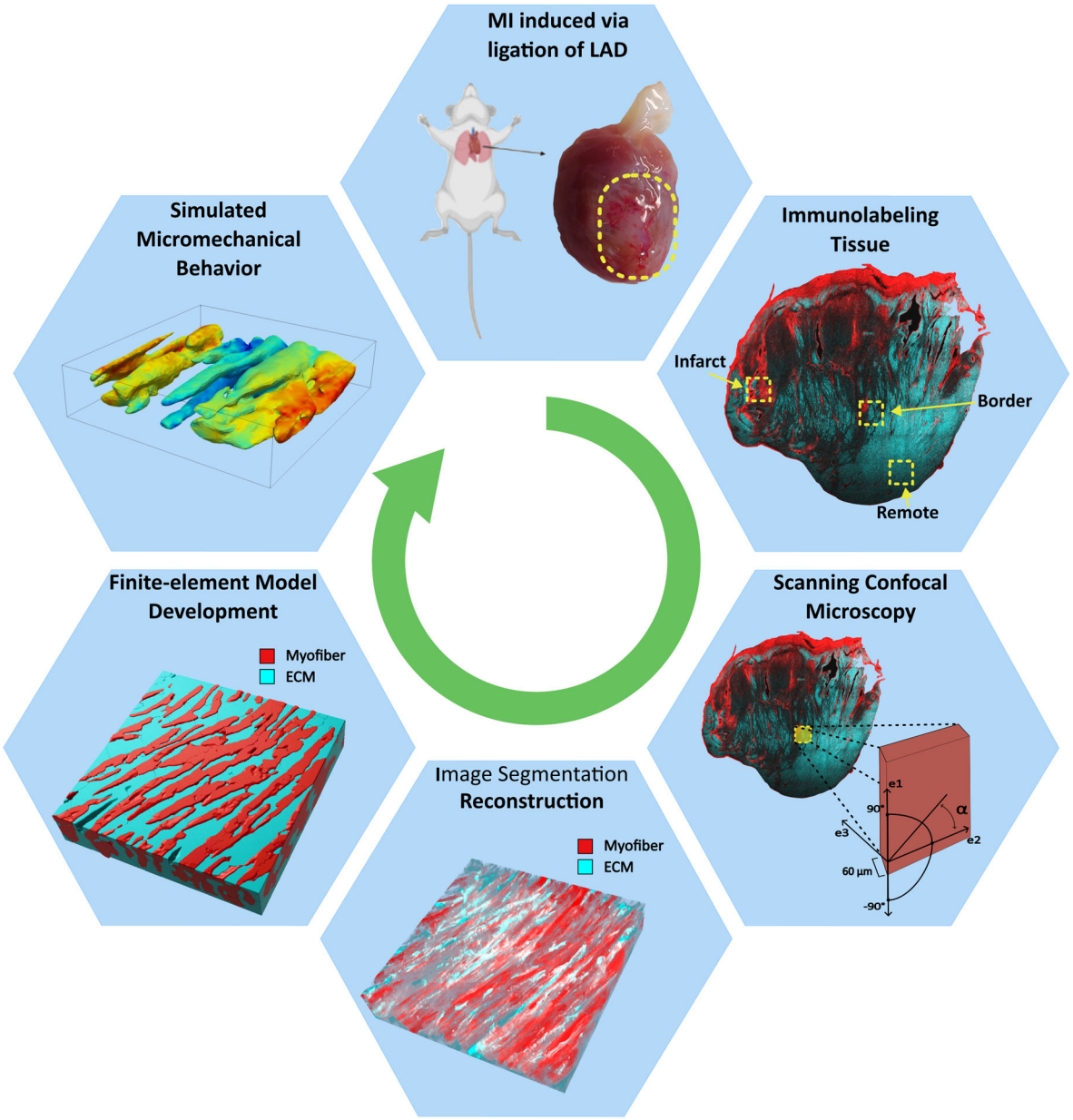

Fig. 1.

Micro-structurally accurate finite-element models of the infarcted LV myocardium were developed from high-resolution imaging. The precise image segmentation process allowed for the identification of myocyte and extracellular matrix regions of the tissue, resulting in a model capable of estimating cellular-level regional kinematic behavior. LAD: left anterior descending artery; ECM: extracellular matrix; α: denotes fiber angle.

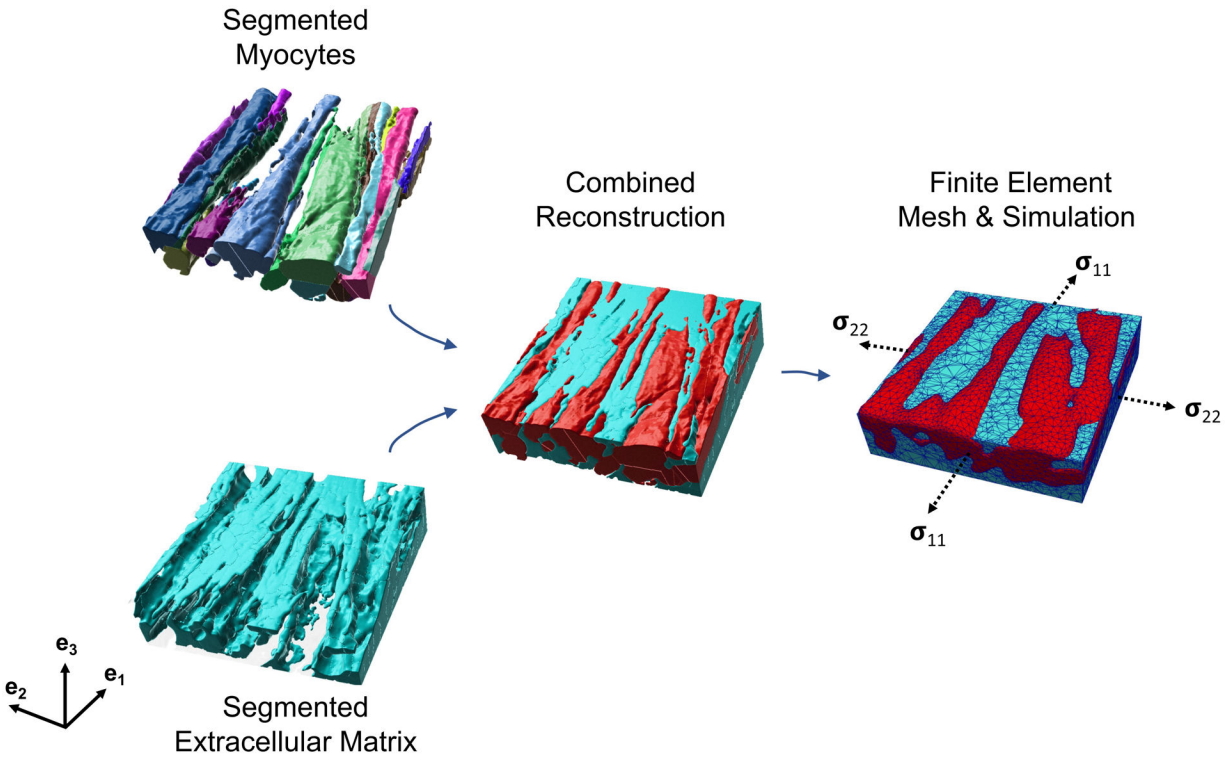

Fig. 2.

Myocytes and the extracellular matrix (ECM) were segmented from high-resolution imaging data. The combined reconstruction was meshed to develop a finite-element representation of the myocardium sample consisting of separate myocyte and ECM regions. The 4-wk post-MI segmentation and model are shown here. The dashed arrows indicate the faces upon which the stress boundary condition was applied. The $\mathbf{e_1}$ and $\mathbf{e_2}$ directions are aligned with the edges of the model.

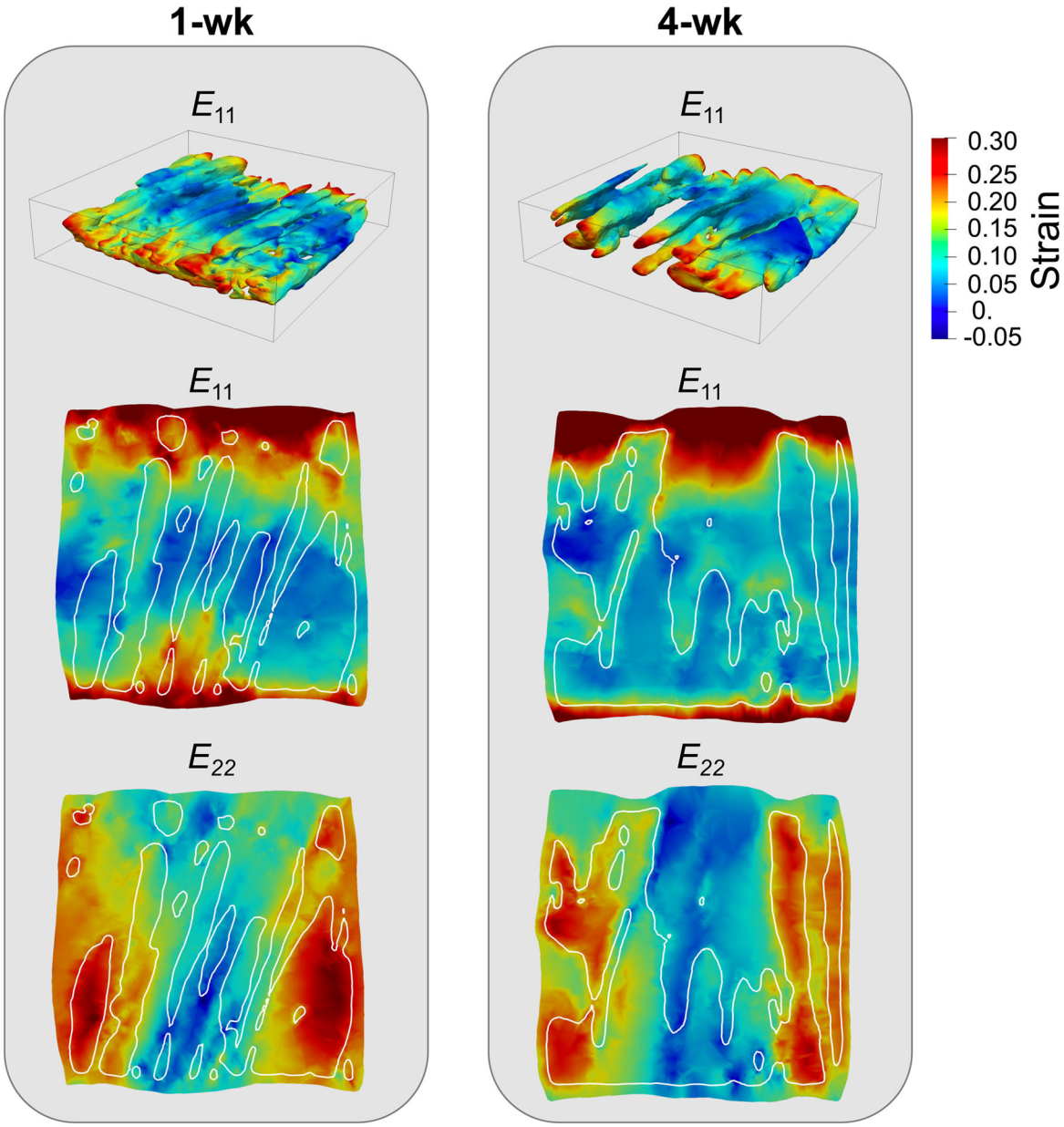

Fig. 3.

3-D visualization of E_{11} in the myofibers (top row) and 2-D cross-sections (second and third rows) of E_{11} and E_{22} at the maximum stress state in the myofiber and ECM regions at the 1-wk and 4-wk post-MI timepoints. The area within the white outlines in the 2-D cross-sections indicated the location of myofibers.

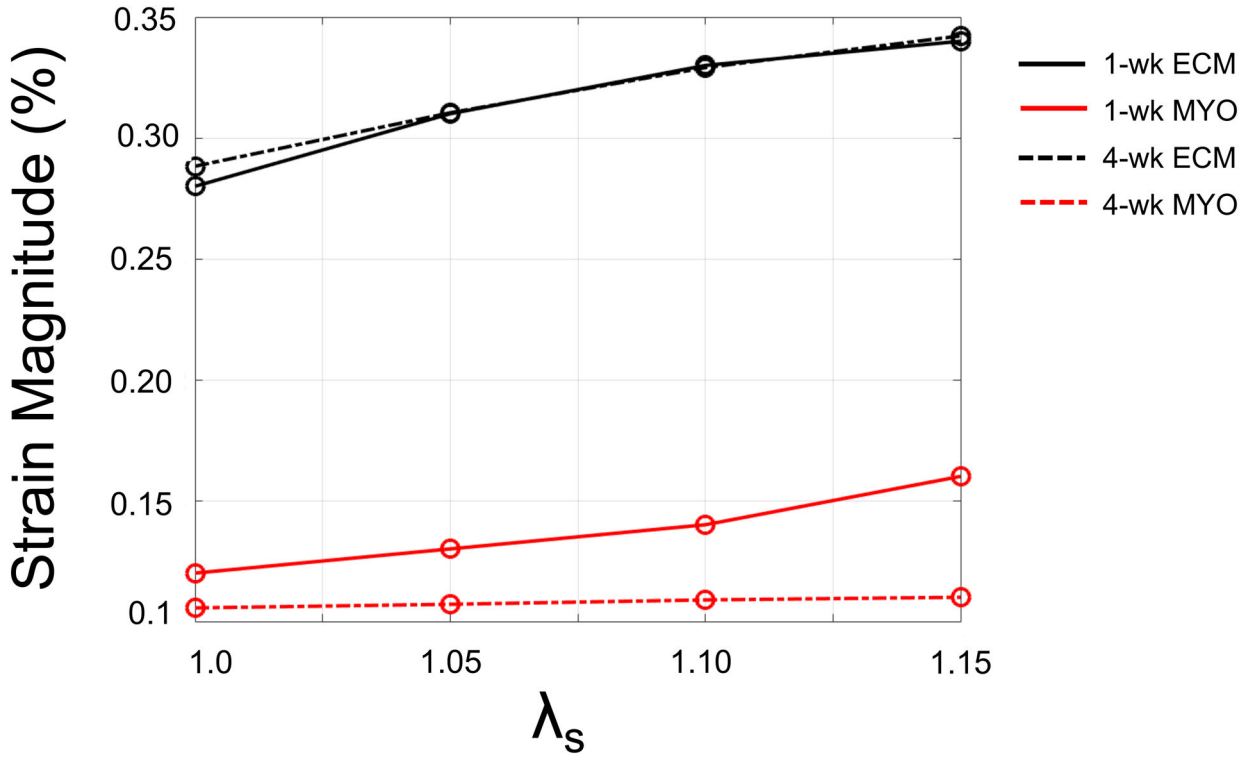

Fig. 4.

Volume-averaged strain magnitude in the myocyte (MYO) and extracellular matrix (ECM) regions as a function of collagen slack stretch (λ_s).